PERSPECTIVE

Check for updates

Interfacial characterization in solid-state lithium metal batteries: advances in temporal, spatial, and energy resolution

Anchun Tang,[a] Minsi Li,*[b] Xueliang Sun*[ac] and Weihan Li [ID] *[a]

All-solid-state lithium metal batteries (ASSLMBs) are widely regarded as promising candidates for next-generation energy storage systems due to their high energy density and intrinsic safety. However, the full realization of their performance potential is significantly hindered by critical challenges at the solid–solid interfaces between electrodes and solid-state electrolytes (SSEs). The interfaces are typically buried within the cell architecture, exhibit substantial chemical heterogeneity, and undergo dynamic evolution across a wide range of spatial and temporal scales, posing formidable obstacles to conventional characterization techniques. In this Perspective, we systematically examine the inherent difficulties in probing solid-state battery interfaces and highlight recent advances in temporal-, spatial-, and energy-resolved characterization methods. Looking forward, the integration of multidimensional analytical platforms with cell configurations tailored for realistic operating conditions will be critical for unravelling interfacial mechanisms, advancing interface engineering, and accelerating the development of high energy-density solid-state batteries.

Broader context

Decarbonizing energy systems demands breakthroughs in electrochemical storage that combine high energy density with uncompromising safety. All-solid-state lithium metal batteries (ASSLMBs) have emerged as one of the most promising solutions, yet their progress is ultimately dictated by the stability and functionality of buried solid–solid interfaces. Advanced characterization methods are therefore indispensable for unveiling these hidden processes. Recent progress in time-, spatial-, and energy-resolved approaches has greatly improved the ability to probe dynamic interfacial phenomena with unprecedented resolution. By capturing interfacial transport, reaction pathways, and mechanical evolution across multiple dimensions, these approaches provide mechanistic insights that directly guide rational interface design. Continued advances in such multidimensional characterization will be essential for translating interfacial understanding into practical design rules, thereby accelerating the reliable deployment of ASSLMB technologies for sustainable energy storage.

1. Introduction

All-solid-state lithium metal batteries (ASSLMBs) are widely recognized as promising candidates for next-generation energy storage systems.[1] As illustrated in Fig. 1, the roadmap delineates the evolution from conventional liquid-electrolyte lithium-ion batteries to solid-state systems. Replacing flammable, leakage-prone liquid electrolytes with solid-state electrolytes (SSEs) yields markedly improved thermal stability and reduced risk of combustion.[2] The adoption of SSEs further enables the safe utilization of lithium metal anodes (theoretical capacity: 3860 mA h g^{-1}; electrochemical potential: -3.04 V $vs.$ SHE), paving the way for energy densities >500 Wh kg^{-1}.[3–5] Furthermore, many inorganic SSEs function as single-ion conductors, supporting fast charge/discharge rates and facilitating the use of high-capacity electrode materials. In addition to enhanced safety and energy metrics, ASSLMBs offer distinct advantages in low-temperature environments.[6] Unlike liquid electrolytes, which often suffer from increased viscosity and ion mobility loss at sub-zero temperatures, certain SSEs retain stable ionic conductivity and interfacial integrity, thereby enabling reliable operation in cold climates and aerospace applications.[7] These attributes collectively underpin the technological potential of ASSLMBs and motivate intensive research into their practical realization.

However, ASSLMBs still face persistent and fundamental challenges at the solid–solid interfaces between electrodes and

^{a} *Eastern Institute for Advanced Study, Ningbo Institute of Digital Twin, Zhejiang Key Laboratory of All-Solid-State Battery, Ningbo Key Laboratory of All-Solid-State Battery, Eastern Institute of Technology, Ningbo, Zhejiang, 315200, China. E-mail: xsun@eitech.edu.cn, whli@eitech.edu.cn*

^{b} *Institute of Micro/Nano Materials and Devices, Ningbo University of Technology, Ningbo, Zhejiang 315211, China. E-mail: tjminsi@nbut.edu.cn*

^{c} *Department of Mechanical and Materials Engineering, Western University, London, Ontario, N6A 5B9, Canada*

electrolytes. These interfaces, characterized by their inherent rigidity, poor conformability, and mechanical incompatibility, often suffer from structural discontinuities, void formation, and local stress accumulation.[8–10] Such features critically undermine interfacial stability, impede efficient lithium-ion transport, and accelerate performance degradation over long-term cycling—ultimately becoming a central bottleneck limiting the scalability and commercial viability of ASSLMB technologies.[11–13] The interfacial issues are further exacerbated by the thermodynamic and electrochemical incompatibilities between electrode materials and SSEs, which can induce undesirable side reactions, interphase formation, and space-charge layer (SCL) development.[14] Addressing these intricacies requires not only rational interfacial design but also a deep mechanistic understanding of the coupled electrochemical, chemical, and mechanical behaviour at the buried interfaces.

Advanced characterization techniques are therefore indispensable in probing the interfaces, offering critical insights into interfacial evolution, degradation pathways, and failure mechanisms.

In this Perspective, we highlight the critical role of advanced characterization techniques in enhancing our understanding of solid-state battery interfaces and driving the development of high-performance systems. By improving temporal, spatial, and energy resolution, these techniques provide deeper insights into the dynamic behaviour at interfaces, which are crucial for performance. We also summarize recent strategies for enhancing interfacial resolution, focusing on key methodological advances that allow for distinguishing interfaces inside the cells. We believe that the insights gained from these emerging characterization techniques will be instrumental in optimizing the electrochemical performance of solid-state batteries.

Anchun Tang

Dr Anchun Tang is a Postdoctoral Researcher at the Eastern Institute of Technology (EIT), Ningbo, China. She obtained her PhD degree from the University of Science and Technology Beijing (USTB) in 2025, with one year of joint training (2023–2024) at Nanyang Technological University (NTU), Singapore. Her research focuses on solid-state batteries, layered oxide cathode materials, and synchrotron-based characterization techniques.

Minsi Li

Dr Minsi Li, Professor and Research Fellow at the Ningbo University of Technology, China. She received her BS from the University of Science and Technology of China in 2016 and her PhD from Western University, Canada, in 2021. From 2021 to February 2025, she carried out postdoctoral research at Western University. She joined Ningbo University of Technology in 2025, where she is currently a Research Fellow. Her research centers on the design and synthesis of solid-state electrolyte materials, the development of all-solid-state lithium batteries, and in situ synchrotron characterization.

Xueliang Sun

Dr Xueliang Sun, Chair Professor at the Eastern Institute of Technology (EIT), Ningbo, China, Foreign Member of the Chinese Academy of Engineering, Fellow of the Royal Society of Canada, Fellow of the Canadian Academy of Engineering, Canada Research Chair, and founding Editor-in-Chief of the international journal Electrochemical Energy Reviews (IF ≈ 36). His research focuses on the fundamentals and applications of solid-state batteries, lithium-ion batteries, and fuel cells. In recent years, he has made a series of original contributions to novel halide solid-state electrolytes and their all-solid-state batteries.

Weihan Li

Dr Weihan Li, Associate Professor (independent PI) at the Eastern Institute of Technology (EIT), Ningbo, China. He received a BS from Sichuan University in 2011 and PhD degrees from the University of Science and Technology of China (2016) and Western University, Canada (2023). He has conducted postdoctoral research at Western University and visiting research at the Canadian Light Source. His research focuses on solid-state batteries, lithium (sodium)-ion batteries, and synchrotron-based characterization. In recent years, he has reported a series of original results on novel nitride solid-state electrolytes, the development of all-solid-state batteries, and in situ synchrotron characterization.
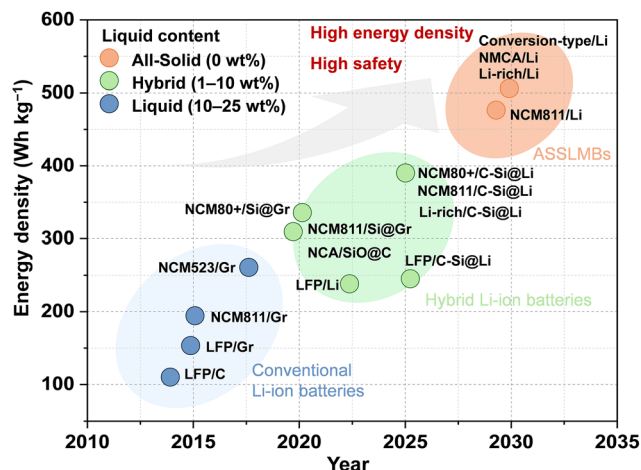
Fig. 1 A roadmap toward high-energy-density and safe battery systems.

2. Fundamental issues and challenges at solid-state lithium metal battery interfaces

2.1 Interfacial issues

ASSLMBs present fundamentally different interfacial characteristics compared to conventional liquid-based lithium-ion batteries. ASSLMBs rely on solid–solid interfaces for ion conduction, but these interfaces lack conformability, causing poor contact, voids, and mechanical stress.[14,15] These interfacial phenomena constitute one of the principal bottlenecks to achieving the full potential of ASSLMBs in practical applications. In the following sections, we systematically discuss the major challenges associated with the cathode–electrolyte and anode–electrolyte interfaces (Fig. 2).

2.1.1 Cathode–electrolyte interface. Chemical and electrochemical instability at the cathode–electrolyte interface represents a major challenge for ASSLMBs employing high-voltage layered oxide cathodes (*e.g.*, $LiNi_{0.8}Mn_{0.1}Co_{0.1}O_2$ or $Li_{1.2}Mn_{0.6}Ni_{0.2}O_2$) paired with sulfide electrolytes such as Li_6PS_5Cl. Thermodynamic incompatibility between these materials can trigger spontaneous chemical decomposition at their boundary, yielding resistive interphases that obstruct Li-ion transport. Under high operating potentials, oxidative breakdown of the sulfide further increases interfacial resistance, driving progressive capacity fade.[16] The resulting unstable interphases not only diminish ionic conductivity but also engender mechanical stresses—arising from local changes in volume and composition—that ultimately undermine both the structural and electrochemical integrity of the interface.

Beyond interfacial chemical and electrochemical degradation, SCL formation imposes a significant electrostatic barrier to Li-ion transport.[17] The electrochemical potential mismatch between the cathode and electrolyte induces lithium-ion depletion near the interface, resulting in charge redistribution and the buildup of an internal electric field. This field opposes further ion migration and exacerbates interfacial impedance.
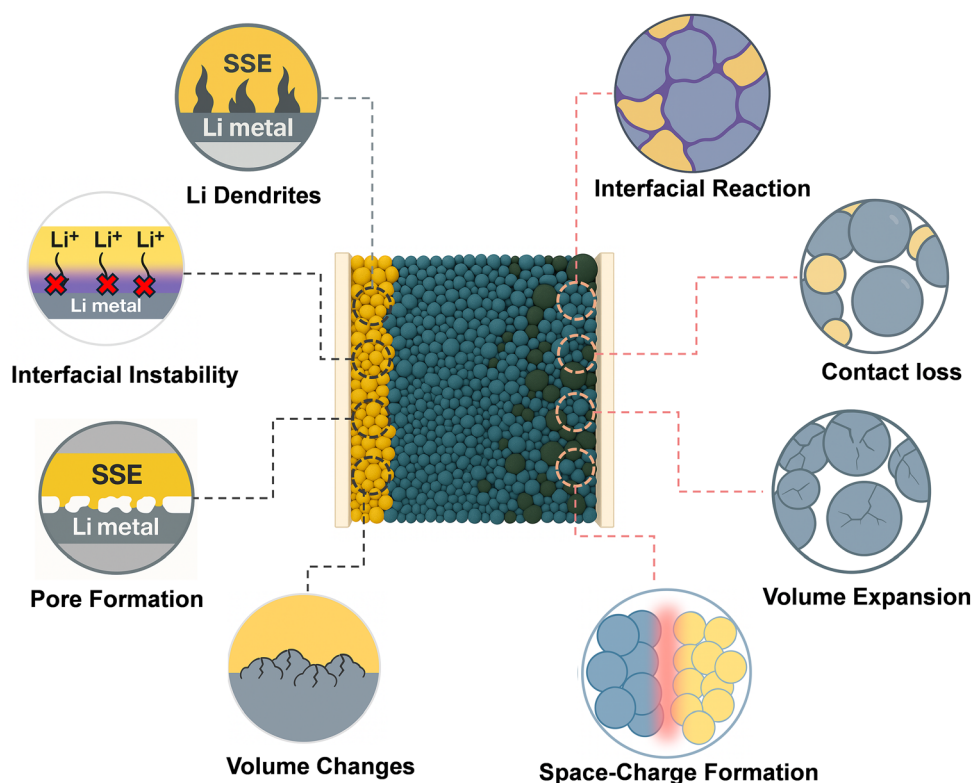

Fig. 2 Interface-related issues in ASSLMBs.

Unlike resistive interphases formed *via* chemical reactions, SCLs originate from intrinsic ion imbalance and persist even in chemically stable systems. Their presence further limits ionic conductivity, promotes transport heterogeneity, and accelerates performance degradation under prolonged cycling.

Finally, the large volume changes that accompany Li insertion and extraction in layered oxides impose severe mechanical strains on the rigid SSEs.[18] Unlike liquid electrolytes, which can accommodate electrode swelling, ceramic electrolytes conform poorly to dynamic volume fluctuations, leading to delamination, cracking, and loss of interfacial contact. Collectively, these chemical, electrostatic, and mechanical phenomena pose formidable obstacles to the development of stable, high-energy-density ASSLMBs.

2.1.2 Anode–electrolyte interface. At the lithium metal–electrolyte interface, interfacial instability in ASSLMBs primarily arises from the spontaneous chemical reduction of SSEs, driven by the high chemical potential of lithium metal. The stability of the lithium metal–electrolyte interface is determined by a complex interplay of thermodynamic, kinetic, and interfacial factors, including the intrinsic reactivity of the SSEs, interfacial contact quality, and the nature of the interphase formed. Stable SSEs such as Li_3N and lithium halides (*e.g.*, LiF, LiCl) form compatible interfaces that facilitate lithium-ion transport while blocking electronic conduction. In contrast, unstable SSEs undergo reduction, forming either solid electrolyte interphases (SEIs)—which are ionically conductive and electronically insulating—or mixed-conductive interphases (MCIs), which sustain parasitic redox reactions that continuously degrade both lithium and the SSEs, undermining long-term cycling stability.[8]

Lithium dendrite growth and interfacial void formation pose additional challenges, typically triggered by inhomogeneous stripping and plating. When local stripping current exceeds lithium replenishment *via* diffusion and deformation, voids emerge, leading to contact loss and current localization.[19] Subsequent plating favors lithium nucleation at void edges, initiating dendrites that propagate along grain boundaries or pre-existing defects, causing delamination, fracture, and internal short circuits. Even in the absence of major defects, surface energy heterogeneity and microstructural irregularities can induce filament growth, highlighting the importance of interfacial morphology in maintaining electrochemical–mechanical stability.

Moreover, the large volume changes during lithium stripping and plating introduce significant mechanical stress.[20] Lithium stripping contracts the Li metal and can detach it from the SSE, whereas plating locally expands Li and imposes stress on the brittle SSE. Unlike liquid electrolytes, SSEs cannot conform to these changes, making them more susceptible to fracture and delamination. The resulting interfacial stress can drive irreversible morphological degradation, including crack initiation and interphase disruption, especially under spatially non-uniform lithium flux and strain distributions.

2.2 Characterization challenges

2.2.1 Intrinsic complexity of the interface

(a) Buried interfaces. In solid-state batteries, the electrode–electrolyte interface is typically buried deep within the multiphase architecture of composite electrodes, existing as an ultrathin layer that is often enveloped by active material particles, solid electrolyte domains, and polymeric binders. This spatial inaccessibility renders conventional surface-sensitive or cross-sectional techniques, such as XPS or SEM, insufficient for directly probing the pristine interface. Furthermore, sample preparation processes involving mechanical polishing or ion milling are not only labor-intensive but also prone to inducing structural reconstruction and chemical alterations, thereby compromising the intrinsic interfacial state. Such buried interfaces pose fundamental challenges for accurately resolving local microstructures, elemental distributions, and oxidation states, while also limiting the ability to monitor their dynamic evolution under realistic operating conditions.

(b) Amorphous and multiphase coexistence. At the solid–solid interfaces of solid-state batteries, the formation of interphases is often accompanied by the emergence of amorphous or nanocrystalline structures as a result of local chemical reactions, interdiffusion, and electrochemical decomposition.[21] Unlike well-ordered crystalline phases, these amorphous regions lack long-range periodicity and exhibit broad, featureless signals in diffraction-based techniques such as X-ray diffraction (XRD) or selected area electron diffraction (SAED), rendering their identification and structural quantification inherently difficult. Moreover, interfacial regions frequently host multiple coexisting phases, including decomposition products (*e.g.*, Li_2S, LiF, metal oxides), metastable intermediates, and gradient composition layers that span only a few nanometers. These structurally and chemically heterogeneous domains often overlap spatially, further complicating signal deconvolution in spectroscopic or imaging-based analyses. The transient and metastable nature of these phases, particularly under dynamic cycling conditions, adds another layer of complexity to their detection.

(c) Light-element enrichment. At the interfaces of solid-state batteries, light elements such as Li, H, B, F, and O are widely present in key reaction products and interphase species.[22] These light elements play indispensable roles in interfacial formation and evolution, including regulating ion flux, interfacial potential distribution, and the structure of SCL. However, due to their intrinsically low atomic numbers, low electron densities, and weak scattering or absorption cross-sections, light elements pose substantial challenges for conventional characterization techniques. These limitations greatly hinder the accurate qualitative, quantitative, and spatial analysis of light-element species at solid–solid interfaces. In addition, light-element species at the interface are often strongly coupled with heavier-element phases, making it difficult to decouple signals or distinguish chemical species using standard spectroscopic methods. For instance, the Li 1s signals of Li_2O, LiOH, and LiF exhibit minimal binding energy differences, posing a challenge for reliable phase identification *via* XPS.

2.2.2 Material sensitivity

(a) Air and moisture sensitivity. Sulfide- and halide-based solid electrolytes are widely recognized as promising candidates for

next-generation ASSLMBs due to their high room-temperature ionic conductivities ($\sim 10^{-3}$–10^{-2} S cm^{-1}). Sulfide electrolytes (*e.g.*, Li_6PS_5Cl, $Li_{10}GeP_2S_{12}$) undergo rapid hydrolysis in humid environments, forming Li_2S, $LiOH$, P–O species, and H_2S gas, often accompanied by crystallographic degradation and a marked decline in ionic conductivity. The accumulation of such decomposition products at the surface or interfaces leads to a substantial increase in interfacial impedance and severely disrupts ion-conduction pathways. Similarly, halide electrolytes (*e.g.*, Li_3InCl_6, Li_3YCl_6, Li_3ErBr_6), though thermally stable, exhibit significant hygroscopicity and hydrolytic reactivity. Their exposure to moisture results in the formation of $LiOH$, HCl, or hydrated halide phases, thereby altering the intrinsic stoichiometry and structural integrity of the electrolyte.[23]

This high environmental sensitivity constrains the processing window and imposes rigorous demands on interfacial characterization, particularly under *in situ* and *operando* conditions. Reasonable probing of the buried interfaces in these systems necessitates the implementation of controlled-atmosphere sample preparation, air-free transfer protocols, and hermetically sealed, vacuum-compatible measurement platforms to preserve the native chemical states and mitigate beam- or atmosphere-induced artifacts.

(b) Beam-induced damage. SSEs often exhibit significant structural and chemical instability under high-energy electron or X-ray irradiation, reflecting their inherent beam sensitivity. At the atomic scale, these materials often possess inherently fragile frameworks and contain volatile or easily reducible anionic species (*e.g.*, S^{2-}, Cl^-, Br^-), which can undergo beam-induced amorphization, anion migration, gas-phase by-product release, or even local phase transitions. These effects collectively contribute to structural distortion and chemical state deviation in the interfacial regions. For instance, in transmission electron microscopy (TEM) and scanning transmission electron microscopy (STEM) coupled with EELS, sulfide-based electrolytes such as Li_6PS_5Cl are prone to sulfur migration and volatilization under electron beam exposure, leading to localized compositional inhomogeneity and lattice degradation.[24] Beam-induced damage can occur on very short time scales—on the order of milliseconds—and remains significant even under low-dose conditions, severely limiting the applicability of high-resolution imaging and spectroscopy for these systems.

2.2.3 *In situ/operando* limitations

(a) In situ cell design. In situ electrochemical cell design is a fundamental prerequisite for reliable interfacial characterization in ASSLMBs under *operando* conditions. Unlike conventional *ex situ* configurations, *in situ* cells must simultaneously ensure electrochemical functionality and meet the stringent spatial, environmental, and geometrical requirements imposed by advanced characterization techniques such as electron microscopy, synchrotron X-ray spectroscopy, and optical or vibrational probes.[11] Compared to liquid-based systems, solid-state batteries impose additional design complexities due to their dense architectures, limited interfacial accessibility, and the necessity of external pressure to maintain interfacial contact.

Electrode–electrolyte interfaces are often deeply embedded within composite electrodes and frequently composed of beam- or air-sensitive materials, necessitating robust sealing and precise sample positioning. Furthermore, the lack of interfacial fluidity inherent to solid–solid contacts necessitates the application of external mechanical pressure to sustain intimate interfacial contact during electrochemical cycling.[25,26] This imposes strict requirements on mechanical integration, including stable and uniform pressure-loading mechanisms and structural compatibility with high-resolution, beamline-based instrumentation. In addition, the establishment of standardized *in situ/operando* cell architectures is essential for achieving experimental reproducibility and enabling meaningful cross-study data comparison, thereby promoting the generation of universally comparable interfacial insights across different characterization platforms.[27]

(b) Kinetic–temporal mismatch. In situ characterization aims to track the dynamic evolution of interfacial structure and chemistry under realistic battery operating conditions. However, critical interfacial events often occur on extremely short time-scales, creating a mismatch between reaction kinetics and the temporal resolution of current techniques. Representative processes—such as lithium dendrite nucleation and penetration, redox-induced local phase transitions, and stress-driven microcrack formation—can be triggered within sub-second or even millisecond intervals, particularly under non-equilibrium conditions such as high current densities, temperature fluctuations, or sudden polarization shifts.[28] However, most *in situ* methods remain constrained by limited acquisition speed, prolonged scan durations, or signal optimization requirements, making it difficult to capture transient events with sufficient temporal fidelity. This kinetic–temporal mismatch not only hampers accurate reconstruction of fast interfacial processes, but also poses substantial challenges for elucidating reaction pathways and validating theoretical models.

(c) Multiscale and multidimensional complexity. Across spatial scales, interfacial behaviour in solid-state batteries span from atomic-scale events—such as point defect formation, localized redox reactions, and lattice distortions—to mesoscale processes involving grain boundaries, phase segregation, and interfacial heterogeneity, and ultimately to macroscale manifestations including mechanical deformation and electrode-level volumetric changes.[29,30] These nested structural hierarchies collectively govern the electrochemical, mechanical, and transport behaviour of the system. Critically, solid-state interfaces are inherently governed by coupled chemo–electro–mechanical fields, resulting in tightly entangled experimental observables. The simultaneous evolution of multiple parameters, compounded by spatial heterogeneity and the buried nature of interfaces, renders mechanistic decoupling extremely challenging. Current *in situ* techniques often struggle to disentangle and quantitatively resolve the coupled multiscale, multi-dimensional, and multi-physics processes that govern interfacial behaviour during cycling.

3. Temporal resolution

Interfacial phenomena in ASSLMBs constitute a series of highly coupled and dynamically evolving processes, including electrochemical reactions, structural rearrangements, chemical phase transitions, stress accumulation, and interfacial degradation. These interfacial processes span a wide range of temporal scales, encompassing ultrafast electron dynamics and bond cleavage on the picosecond to nanosecond timescale, ion migration and SEI/cathode electrolyte interphase (CEI) reconstruction over milliseconds to minutes, and long-term interfacial delamination processes occurring over hours or longer.[11,31,32] Under extreme operating conditions such as high voltage, fast charging, and thick electrode configurations, these interfacial phenomena often exhibit pronounced time dependence and strong non-equilibrium characteristics, constituting key contributors to capacity fading, internal short circuits, and thermal runaway. For instance, the formation of the SEI or CEI typically initiates within seconds to minutes during the first charge, with reaction pathways constrained by scan rates and interfacial ion concentration gradients. The long-term stability of these interphases is further dictated by the migration and reorganization of interfacial species over subsequent cycles. Without time-resolved *in situ* or *operando* characterization techniques capable of capturing these transient transformations and their critical time windows, it becomes exceedingly difficult to elucidate failure mechanisms or accurately evaluate the intrinsic performance of interfacial materials.

The core of temporal resolution lies in minimizing the acquisition time of individual frames, synchronizing with the dynamic response of materials, and simultaneously retaining sufficient spatial and energy resolution. Fig. 3 summarizes the temporal resolution of recently developed characterization techniques. Primarily, the combination of synchrotron radiation sources with high-speed two-dimensional detectors has markedly improved the acquisition rate, enabling sub-second continuous scanning and, in state-of-the-art implementations, sub-millisecond to microsecond time resolution. This is well suited for real-time tracking of interfacial redox reactions, changes in coordination environments, and phase transitions.[33-35] In addition to improvements in the light source itself, optimizing the experimental configuration is equally critical. The design of *in situ* electrochemical cells can reduce signal attenuation and response delay. To further enhance the temporal resolution for probing the evolution of structures, multi-point parallel acquisition strategies enable simultaneous data collection across imaging, energy, and angular dimensions. Furthermore, when interfacial reactions exhibit distinct electrochemical features, non-uniform time-interval sampling strategies can be employed to intensify data collection during critical time windows, thereby enhancing experimental efficiency.

Building upon these methodological advancements, time-resolved characterization techniques have been increasingly applied to ASSLMBs, offering unprecedented insights into their multiscale interfacial evolution.[20,36-45] To investigate the dynamic redox behaviour of high-entropy oxide cathodes,
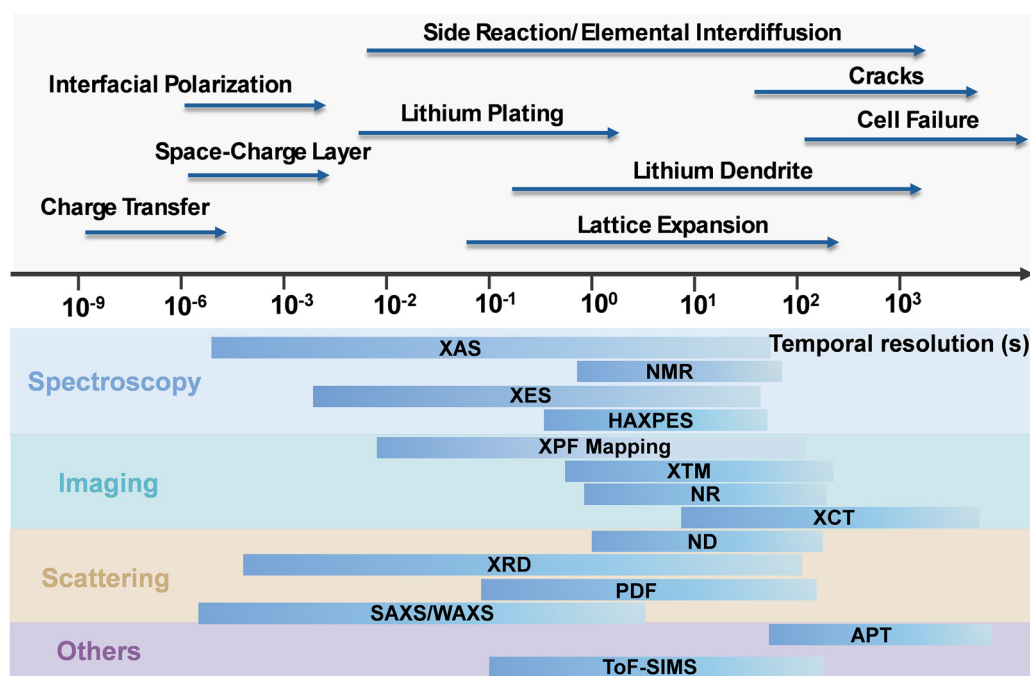

Fig. 3 Comparison of the temporal resolution (unit: seconds) among different characterization techniques. The techniques include: X-ray absorption spectroscopy (XAS); nuclear magnetic resonance spectroscopy (NMR); X-ray emission spectroscopy (XES); hard X-ray photoelectron spectroscopy (HAXPES); X-ray fluorescence mapping (XRF mapping); transmission X-ray microscopy (TXM); neutron radiography (NR); X-ray computed tomography (XCT); neutron diffraction (ND); X-ray diffraction (XRD); pair distribution function (PDF); small-angle/wide-angle X-ray scattering (SAXS/WAXS); atom probe tomography (APT); time-of-flight secondary ion mass spectrometry (ToF-SIMS).

Luo and co-workers[44] utilized *operando* quick-scanning X-ray absorption spectroscopy (quick-XAS) to study a Co-free spinel-type $(CrMnFeNiCu)_3O_4$ material during lithium insertion and extraction. With time-resolved K-edge tracking of Mn, Fe, Cu, Ni, and Cr, the study revealed a stepwise and element-specific redox sequence: Mn and Cu were reduced at the early stage of discharge, followed by Fe and Ni, while Cr exhibited delayed reduction that contributed significantly at lower voltages. Upon charging, Mn and Cr were preferentially reoxidized, whereas Cu remained largely in the metallic state, indicating its irreversible nature. Nomura *et al.*[45] applied a time-resolved *operando* STEM-EELS approach to track nanoscale lithium dynamics across $LiCoO_2$/LASGTP interfaces. By acquiring 157 sequential Li K-edge EELS maps at 12-second intervals, they achieved temporal resolution sufficient to monitor lithiation/delithiation in real time during galvanostatic cycling. Their results showed that Li^+ deintercalation began at grain boundaries, Li redistributed directionally under open-circuit conditions due to internal chemical potential gradients, and cycling induced nonmonotonic Li profiles indicative of local transport bottlenecks. By leveraging time-resolved *operando* XCT with 3-minute intervals per tomogram, Ning *et al.*[20] systematically investigated the initiation and propagation of lithium dendrites in symmetric $Li|Li_6PS_5Cl|Li$ solid-state cells, aiming to establish the correlation between interfacial instability and mechanical failure. The study revealed that dendrite nucleation originates from localized lithium deposition in subsurface pores of the SSEs, leading to stress accumulation and microcrack formation. Rather than advancing from crack tips, dendrites propagate *via* lithium infilling within pre-existing cracks, promoting a wedge-opening fracture mode that ultimately causes cell failure.

4. Spatial resolution

In ASSLMBs, the electrode–electrolyte interface spans multiple spatial scales, ranging from atomic-level features—such as local coordination environments, bond reconstruction, and point defect evolution—to nanoscale phenomena including SCL modulation, interfacial phase stability, and ion deposition behaviour.[46] At the microscale, interfacial processes further manifest as interface roughening, particle debonding, and pore formation, collectively affecting the mechanical integrity and structural uniformity of the electrode at the macroscopic level. Taking interfacial ion transport as an example, the migration pathways and transport efficiency are regulated by multiple intertwined factors, including crystallographic order, defect distributions, interphase structure, charge accumulation, and contact morphology—spanning a broad range of spatial scales and exhibiting strong hierarchical coupling. Therefore, a comprehensive characterization framework that integrates multi-resolution and cross-scale capabilities is essential for elucidating interfacial mechanisms in ASSLMBs.[47] Fig. 4 summarizes representative spatially resolved characterization techniques commonly employed in interface analysis. Even within the same class of techniques, the attainable spatial resolution can vary significantly depending on the instrumentation platform and the nature of the radiation source.

To overcome the spatial resolution limitations of conventional XAS, recent advances integrating it with TXM have enabled nanoscale mapping of chemical states.[11,48–54] Lou *et al.*[52] used *operando* TXM with spatially resolved XANES to track Ni K-edge shifts in individual NCM particles during charging, revealing a surface-to-core delithiation pathway. Despite interfacial discontinuities, near-complete delithiation was achieved *via* coupled potential and concentration-driven diffusion. Wang *et al.*[53] utilized *in situ* TXM-based 5D XANES tomography to visualize delithiation in single $LiFePO_4$ particles, revealing a transition from anisotropic to isotropic phase propagation. The internal core–shell structure and two-phase coexistence were clearly resolved, showing vertically sliced XANES spectra that confirm distinct $LiFePO_4$ and $FePO_4$ phases without intermediates. In addition, by tuning the incident angle of X-rays to reduce the probing depth, the signal contribution from interfacial chemical and structural information can be significantly enhanced, thereby improving interfacial sensitivity. Li *et al.*[54] optimized the incident angle to $\sim 3°$ to investigate the $Li_9N_2Cl_3$/Li metal interface using operando SXRD and XANES. The results revealed no emergence of new crystalline phases or distinct absorption features during prolonged contact and Li plating/stripping, thereby confirming the chemical stability and excellent lithium compatibility of this solid electrolyte at the interface.

Among high-resolution imaging techniques, cryogenic TEM (cryo-TEM) has emerged as a powerful approach for probing beam-sensitive materials and metastable interphases with atomic-level precision. By vitrifying samples below -170 °C and applying low-dose imaging, cryo-TEM mitigates beam-induced damage and preserves intrinsic interfacial structure. This technique is particularly effective for directly visualizing nanostructured SEI/CEI layers and solid–solid interphases.[46,55–59] Wang *et al.*[59] used cryo-TEM to examine the CEI in $Li|PCL-CSE20|NCM523$ solid-state batteries. The PCL-CSE20 electrolyte, composed of $Li_{6.5}La_3Zr_{1.5}Ta_{0.5}O_{12}$ (LLZTO) nanoparticles, a PCL matrix, and LiFSI, formed a well-defined bilayer structure with a crystalline LiF/Li_2O-rich inner layer and a polymer and amorphous inorganic outer layer. Sun *et al.*[46] employed cryo-TEM to directly visualize lithium nucleation and growth inside Li_3PS_4 SSEs, revealing that internal crystalline defects serve as nucleation sites and drive dendrite formation within the bulk rather than at the Li/SSE interface. Cheng *et al.*[56] used cryo-TEM to investigate the structural and chemical characteristics of the Li/LiPON interface. The study revealed concentration gradients of nitrogen and phosphorus within the lithium metal and identified an interphase layer less than 80 nm thick, composed of Li_2O, Li_3N, and Li_3PO_4, arranged in a distinct multilayer mosaic-like distribution. These studies highlight cryo-TEM's unique capability to resolve fine interfacial architectures and compositional inhomogeneities at the atomic scale. However, cryo-TEM requires complex cryogenic sample preparation and its inherently localized field
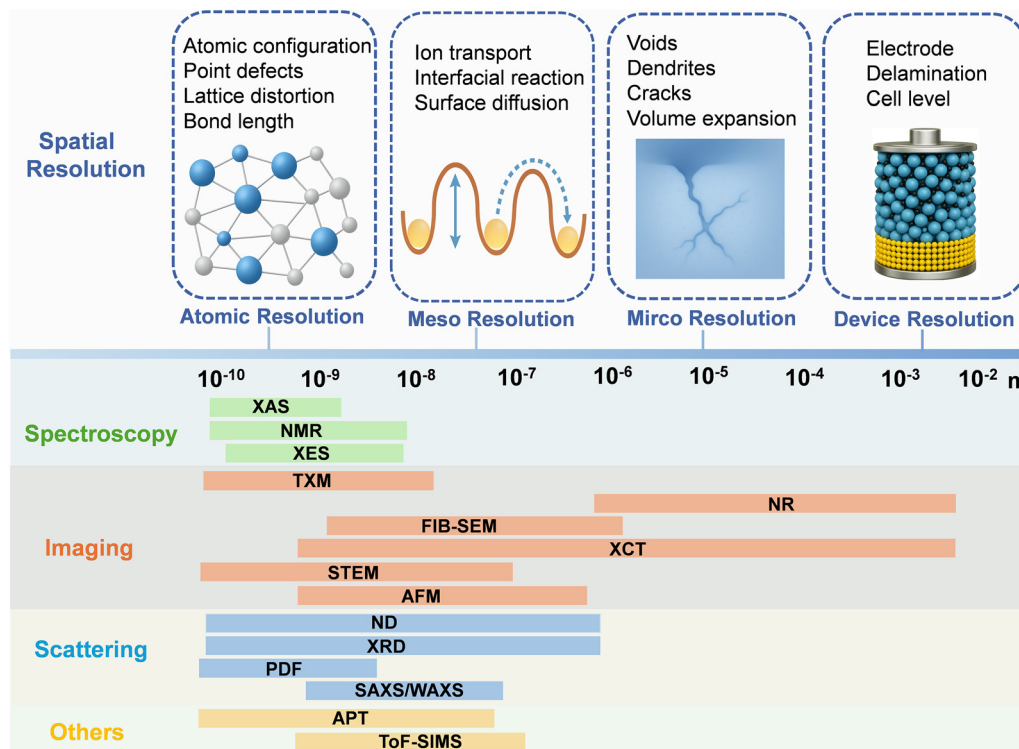
Fig. 4 Comparison of the spatial resolution (unit: meters) of various characterization techniques. The techniques include: XAS; NMR; XES; HAXPES; XRF mapping; TXM; NR; focused ion beam-scanning electron microscopy (FIB-SEM); XCT; scanning transmission electron microscopy (STEM); atomic force microscopy (AFM); ND; XRD; PDF; SAXS/WAXS; APT; ToF-SIMS.

of view limits the number of probed regions, thereby constraining both statistical representativeness and the ability to capture mesoscale heterogeneity within the electrode–electrolyte interface.

To access the three-dimensional morphology and dynamic evolution of interfaces within bulk electrodes and full cells, XCT has emerged as a powerful alternative. Benefiting from recent synchrotron advancements, XCT now covers a wide spatial resolution range—from ∼30 nm to hundreds of micrometres—depending on source brilliance and imaging mode. While this wide tunability enables versatile imaging, XCT inherently involves a trade-off between spatial resolution and penetration depth, as achieving higher resolution typically requires higher-energy or smaller-field imaging. Accordingly, the imaging conditions must be carefully optimized to match specific experimental objectives and sample characteristics. The superior penetration depth and 3D reconstruction capability of XCT make it especially suitable for *in situ* visualization of lithium deposition, interfacial void formation, phase and microstructural evolution, and component distribution.[60–67] For instance, McDowell *et al.*[65] employed *operando* XCT to study Li|Li$_{10}$SnP$_2$S$_{12}$|Li symmetric cells, clearly capturing the formation of voids during lithium stripping and identifying current constriction—resulting from interfacial contact loss—as a key factor in cell failure. They also observed global volume changes caused by partial molar volume mismatch between the electrodes, thereby revealing the underlying

mechanism of interfacial degradation. In another study, Sadd *et al.*[66] developed *operando* XCT with high temporal resolution to investigate lithium morphology evolution and the formation of inactive lithium (''dead Li'') under various current densities, shedding light on structural origins of low Coulombic efficiency. Beyond probing lithium dendrites, XCT has also been applied to investigate the structural characteristics of SSEs. Li *et al.*[67] utilized XCT to reveal the critical impact of grain-boundary porosity on the performance of Li$_3$InCl$_6$. Cold-pressed samples exhibited abundant intergranular voids, which impeded lithium-ion transport and facilitated dendrite growth, whereas hot pressing significantly reduced porosity and enhanced interparticle connectivity. The 3D reconstructions provided by XCT clearly demonstrated that increased relative density correlates with improved ionic conductivity and enhanced dendrite suppression capability.

5. Energy resolution

The electrode–electrolyte interface in ASSLMBs acts as a multifunctional domain that governs ion/electron transport and mediates complex interfacial reactions and structural transformations.[68] This interfacial region is typically enriched with light elements such as Li, O, F, S and P.[69] The low binding energies, narrow chemical shifts, and dense electronic states of these elements render their spectroscopic features highly prone

to convolution in complex environments. Moreover, under *in situ* or *operando* conditions, additional challenges arise from limited sample stability and the intrinsic trade-offs among spatial, temporal, and energy resolution, which further complicate the detection and differentiation of weak interfacial signals. These features significantly increase the complexity of spectral interpretation. Consequently, key information related to valence state transitions, electronic structure evolution, and local coordination changes often appears as subtle spectroscopic features, such as small chemical shifts or edge structure variations within the range of 0.1 to 0.5 eV.[70] Insufficient energy resolution can obscure these interfacial features, as they are often masked by background noise or by the dominant spectral contributions from bulk components.

To resolve these challenges, advanced spectroscopic methods with high energy resolution and element specificity have become essential for probing buried interfacial chemistry in ASSLMBs.[71] XPS probes the chemical states of elements by measuring the kinetic energy of emitted electrons (Fig. 5(a)). The ultimate resolution is jointly constrained by the photon bandwidth, spectrometer and detector performance, electronic stability, and the intrinsic lifetime broadening of core states. Laboratory monochromatic XPS typically achieves a resolution of 0.3–0.5 eV, whereas synchrotron-based HAXPES attains 0.1–0.2 eV at selected photon energies, providing sufficient probing depth to access buried interfaces.[72–76] Leveraging these advantages, Aktekin *et al.*[75] conducted an *operando* HAXPES investigation of the electrochemical decomposition of Li_6PS_5Cl at the interface between the nickel film and Li_6PS_5Cl. The high energy resolution (~ 0.2 eV) facilitated precise deconvolution of

spectral features, allowing unambiguous identification of decomposition products such as Li_2S and Li_2O, which emerged at specific potentials (1.75–1.0 V *vs.* Li^+/Li) and exhibited distinct chemical shifts and shoulder features. Building upon this approach, Dubey *et al.*[76] employed HAXPES with slightly reduced energy resolution but significantly greater probing depth (~ 17–19 nm), enabling comprehensive characterization of interfacial species including Li_2O, $LiOH$, and Li_2CO_3 on variously treated $Li_7La_3Zr_2O_{12}$ (LLZO) surfaces.

High-energy-resolution fluorescence-detected XANES (HERFD-XANES) captures fluorescence with high spectral resolution to suppress core-hole lifetime broadening, delivering sub-eV energy resolution (commonly ~ 0.3–0.8 eV, edge-dependent) and heightened sensitivity to subtle electronic and structural signatures.[77–79] It is applied mainly in the hard X-ray regime. Soft X-ray absorption spectroscopy (sXAS) provides superior surface sensitivity and high energy resolution, making it particularly powerful for probing light elements such as O, F at battery interfaces. However, in systems involving multiple overlapping redox processes, the resulting spectra often suffer from feature convolution, making it difficult to resolve individual excitation contributions. In contrast, resonant inelastic X-ray scattering (RIXS) captures the energy loss of emitted photons following incident photon excitation, generating a two-dimensional map of incident *versus* emitted photon energies that enables higher-dimensional electronic structure analysis (Fig. 5(a)).[80–82] The energy resolution of RIXS can exceed 0.1 eV, and at state-of-the-art soft X-ray beamlines, it can reach below 0.02 eV. These capabilities enable the direct probing of low-energy excitations, such as phonons, magnons, orbital
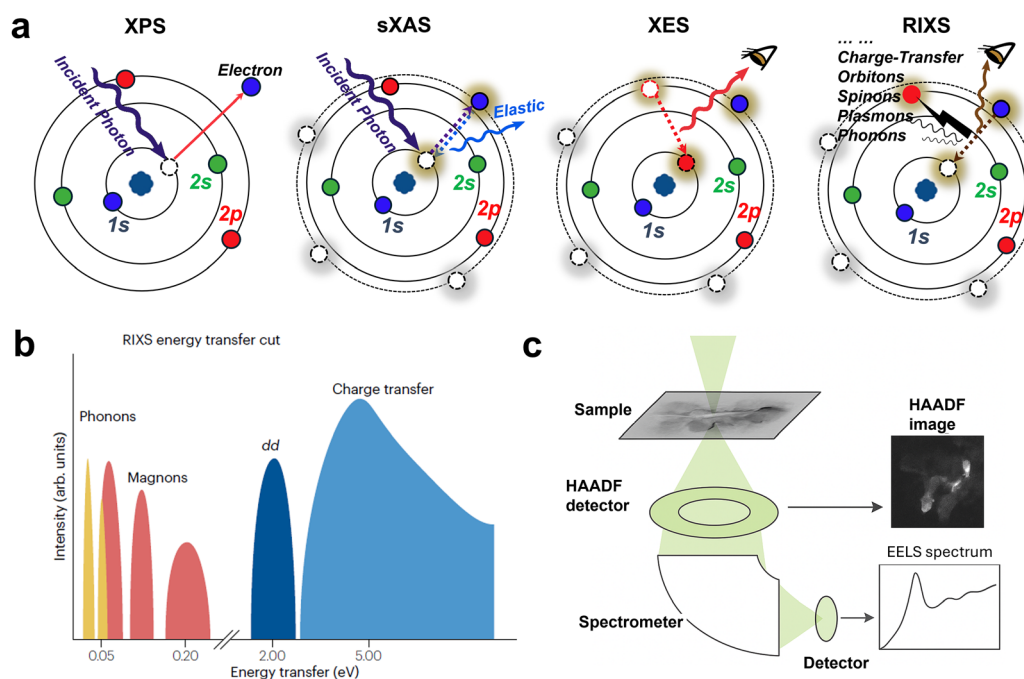

Fig. 5 (a) The simplified atomic model of XPS, sXAS, X-ray emission spectroscopy (XES), and RIXS. Reprinted with permission from ref.[80] Copyright 2018, Elsevier Ltd. (b) Types of excitations in 2p–3d RIXS experiments. Reprinted with permission from ref.[82] Copyright 2024, Springer Nature.(c) Schematic illustration of STEM-EELS measurement. Reprinted with permission from ref.[84] Copyright 2015, Royal Society of Chemistry.

transitions, and charge-transfer dynamics (Fig. 5(b)), thereby providing unique and comprehensive insights into excited-state behaviour, strong electronic correlations, and electron–lattice coupling in materials.[82] In recent years, RIXS has been widely employed to investigate anionic redox processes, and although its application in ASSLMBs is still limited, it shows considerable promise for elucidating interfacial reaction products.

Compared with XAS, which probes unoccupied electronic states *via* photon absorption with typical sub-eV energy resolution, EELS follows the same dipole selection rules in the small-q limit but exploits inelastically scattered electrons (Fig. 5(c)), thereby enabling comparable information on oxidation states and coordination environments with the added advantage of high spatial resolution in the electron microscope.[83,84] With monochromated electron sources and improved spectrometers, EELS achieves ~ 0.1 eV resolution in the low-loss regime, and core-loss measurements routinely extend to several-keV edges (heavier elements commonly probed *via* L/M edges), broadening elemental coverage.[71] EELS offers broader elemental accessibility and enhanced sensitivity to low-Z elements, including Li, Be, and B, which are often inaccessible or extremely challenging to detect *via* XAS.[85] Notably, the Li K-edge (~ 55 eV) is readily accessible in EELS, enabling spatially resolved analysis of lithium-ion distribution, interfacial transport pathways, and SEI composition. These capabilities render EELS a powerful and complementary technique to XAS for elucidating lithium-related phenomena in ASSLMBs.[86–89] Lee *et al.*[89] systematically investigated the effect of crystallographic orientation on interfacial thermal stability in epitaxially grown $Li(Ni_{1/3}Co_{1/3}Mn_{1/3})O_2$ (NCM)/$Li_{3x}La_{(2/3)-x}\square_{(1/3)-2x}TiO_3$ (LLTO) heterostructures using *in situ* STEM-EELS. The Li EELS mapping revealed lithium-ion migration from NCM into LLTO, which initiated at approximately 100 °C in the open-channel interface but was delayed to around 400 °C in the closed-channel configuration.

6. Summary and future perspectives

The structure and evolution of solid–solid interfaces in solid-state batteries play a decisive role in determining overall device performance. This Perspective systematically reviews the key technical challenges in interfacial characterization and highlights recent advances in time-, spatial-, and energy-resolved approaches. To gain a more comprehensive understanding of interfacial dynamics, it is crucial to integrate these three dimensions in practical research. Multimodal strategies enable simultaneous visualization of morphological evolution, chemical reactions, and charge transfer processes. Collectively, these complementary dimensions bridge the gap between fast interfacial reactions, nanoscale structure evolution, and macroscopic electrochemical performance, guiding the rational design of stable and high-performance solid-state interfaces.

Future advances in interfacial design and characterization are anticipated to focus on the following directions:

First, the design paradigm for solid–solid interfaces should transition from passive accommodation to proactive and adaptive regulation. This shift necessitates the integration of multifunctional strategies—including electrochemical window alignment, SCL engineering, interfacial chemistry control, and mechanical stress management—to establish a dynamic yet robust interfacial environment. Such proactive design enables the suppression of parasitic reactions, alleviation of space-charge accumulation, and mitigation of chemo-mechanical mismatch, addressing the key interfacial degradation pathways in ASSLMBs. By achieving a synergistic balance between structural integrity, ionic/electronic transport, and chemical compatibility, future interface designs will be better equipped to address the complex challenges of next-generation ASSLMBs. Ultimately, advancing our fundamental understanding and regulatory capabilities at the solid–solid interface is essential for unlocking the full potential of all-solid-state energy storage systems in practical and scalable applications.

Second, it is essential to develop advanced *in situ* and *operando* characterization platforms that offer simultaneous high temporal, spatial, and energy resolution. These tools must be capable of probing buried interfaces under realistic and often harsh operating conditions to capture interfacial transformations and disentangle dynamic processes occurring under far-from-equilibrium states. By resolving transient phenomena such as interphase formation, Li dendrite nucleation, and stress accumulation in real time, these techniques can reveal the fundamental origins of interfacial degradation and validate mechanistic models that are often inaccessible through conventional *ex situ* characterization. The integration of multimodal and multi-scale measurement techniques, combined with synchronized data acquisition and real-time analysis, will be critical for unveiling the transient structural, chemical, and electronic evolutions that govern interfacial behaviour in ASSLMBs.

Third, the integration of multiple complementary characterization techniques has become increasingly essential. By combining spectroscopic, imaging, and scattering methods, it is possible to probe interfacial evolution from multiple dimensions—including structural configuration, electronic states, and chemical composition—thereby overcoming the inherent limitations of any single technique in spatial or signal resolution. Such integrative approaches enable the cross-validation of results obtained from different modalities and establish direct correlations between structural, chemical, and electrochemical features across multiple length scales. Ultimately, a deeper mechanistic understanding of solid-state interfaces will be the key to guiding rational material design and unlocking the full commercial potential of ASSLMBs.

Fourth, theoretical modeling and data-driven machine learning approaches are expected to play an increasingly critical role in complementing experimental investigations. Atomistic simulations, phase-field modeling, and continuum-scale calculations can provide mechanistic insights into interfacial reactions, ion transport, and stress evolution that are challenging to capture experimentally. Meanwhile, emerging machine-learning

frameworks can accelerate data analysis, pattern recognition, and interfacial descriptor discovery, enabling predictive understanding and inverse design of solid–solid interfaces. The integration of experimental and computational methodologies will thus establish a powerful closed-loop paradigm, in which simulations guide experiments and experimental data refine theoretical models, ultimately enhancing both the efficiency and accuracy of interfacial characterization and design.

Conflicts of interest

The authors declare no competing interests.

Data availability

No primary research results, software or code have been included and no new data were generated or analysed as part of this Perspective.

Acknowledgements

References

1 A. M. Bates, Y. Preger, L. Torres-Castro, K. L. Harrison, S. J. Harris and J. Hewson, *Joule*, 2022, **6**, 742–755.

2 J. Janek and W. G. Zeier, *Nat. Energy*, 2016, **1**, 1–4.

3 S. Kalnaus, N. J. Dudney, A. S. Westover, E. Herbert and S. Hackney, *Science*, 2023, **381**, eabg5998.

4 W. Li, M. Li, H. Ren, J. T. Kim, R. Li, T.-K. Sham and X. Sun, *Energy Environ. Sci.*, 2025, **18**, 4521–4554.

5 A. C. C. Dutra, B. A. Goldmann, M. S. Islam and J. A. Dawson, *Nat. Rev. Mater.*, 2025, **10**, 566–583.

6 P. Lu, Z. Zhou, Z. Xiao, J. Lu, J. Zhang, G. Hu, W. Yan, S. Xia, S. Zhang, Z. Wang, H. Li, C. Wang, F. Wu and X. Sun, *Joule*, 2024, **8**, 635–657.

7 B. Hong, L. Gao, C. Li, G. Lai, J. Zhu, D. Huang, Y. Zuo, W. Yin, M. Sun, S. Zhao, J. Zheng, S. Han and R. Zou, *Nat. Commun.*, 2025, **16**, 143.

8 S. Lou, F. Zhang, C. Fu, M. Chen, Y. Ma, G. Yin and J. Wang, *Adv. Mater.*, 2021, **33**, e2000721.

9 X. Miao, S. Guan, C. Ma, L. Li and C. W. Nan, *Adv. Mater.*, 2023, **35**, e2206402.

10 J. Ahn, H. Lim, J. Ko and J. Cho, *Energy Adv.*, 2024, **3**, 2152–2174.

11 M. B. Dixit, J.-S. Park, P. Kenesei, J. Almer and K. B. Hatzell, *Energy Environ. Sci.*, 2021, **14**, 4672–4711.

12 A. C. C. Dutra, J. A. Quirk, Y. Zhou and J. A. Dawson, *ACS Mater. Lett.*, 2024, **6**, 5039–5047.

13 Y. Guo, Q. Niu, F. Pei, Q. Wang, Y. Zhang, L. Du, Y. Zhang, Y. Zhang, Y. Zhang, L. Fan, Q. Zhang, L. Yuan and Y. Huang, *Energy Environ. Sci.*, 2024, **17**, 1330–1367.

14 A. Banerjee, X. Wang, C. Fang, E. A. Wu and Y. S. Meng, *Chem. Rev.*, 2020, **120**, 6878–6933.

15 Y. Tian, T. Shi, W. D. Richards, J. Li, J. C. Kim, S.-H. Bo and G. Ceder, *Energy Environ. Sci.*, 2017, **10**, 1150–1166.

16 B. Zahiri, A. Patra, C. Kiggins, A. X. B. Yong, E. Ertekin, J. B. Cook and P. V. Braun, *Nat. Mater.*, 2021, **20**, 1392–1400.

17 L. Wang, R. Xie, B. Chen, X. Yu, J. Ma, C. Li, Z. Hu, X. Sun, C. Xu, S. Dong, T. S. Chan, J. Luo, G. Cui and L. Chen, *Nat. Commun.*, 2020, **11**, 5889.

18 N.-Y. Park, H.-U. Lee, T.-Y. Yu, I.-S. Lee, H. Kim, S.-M. Park, H.-G. Jung, Y.-C. Jung and Y.-K. Sun, *Nat. Energy*, 2025, **10**, 479–489.

19 D. Cao, X. Sun, Q. Li, A. Natan, P. Xiang and H. Zhu, *Matter*, 2020, **3**, 57–94.

20 Z. Ning, G. Li, D. L. R. Melvin, Y. Chen, J. Bu, D. Spencer-Jolly, J. Liu, B. Hu, X. Gao, J. Perera, C. Gong, S. D. Pu, S. Zhang, B. Liu, G. O. Hartley, A. J. Bodey, R. I. Todd, P. S. Grant, D. E. J. Armstrong, T. J. Marrow, C. W. Monroe and P. G. Bruce, *Nature*, 2023, **618**, 287–293.

21 F. Ren, Z. Liang, W. Zhao, W. Zuo, M. Lin, Y. Wu, X. Yang, Z. Gong and Y. Yang, *Energy Environ. Sci.*, 2023, **16**, 2579–2590.

22 L. Ye and X. Li, *Nature*, 2021, **593**, 218–222.

23 A. Manthiram, X. Yu and S. Wang, *Nat. Rev. Mater.*, 2017, **2**, 16103.

24 S. Narayanan, U. Ulissi, J. S. Gibson, Y. A. Chart, R. S. Weatherup and M. Pasta, *Nat. Commun.*, 2022, **13**, 7237.

25 J. Gu, Z. Liang, J. Shi and Y. Yang, *Adv. Energy Mater.*, 2022, **13**, 2203153.

26 R. Koerver, W. Zhang, L. de Biasi, S. Schweidler, A. O. Kondrakov, S. Kolling, T. Brezesinski, P. Hartmann, W. G. Zeier and J. Janek, *Energy Environ. Sci.*, 2018, **11**, 2142–2158.

27 S. Puls, E. Nazmutdinova, F. Kalyk, H. M. Woolley, J. F. Thomsen, Z. Cheng, A. Fauchier-Magnan, A. Gautam, M. Gockeln, S.-Y. Ham, M. T. Hasan, M.-G. Jeong, D. Hiraoka, J. S. Kim, T. Kutsch, B. Lelotte, P. Minnmann, V. Miß, K. Motohashi, D. L. Nelson, F. Ooms, F. Piccolo, C. Plank, M. Rosner, S. E. Sandoval, E. Schlautmann, R. Schuster, D. Spencer-Jolly, Y. Sun, B. S. Vishnugopi, R. Zhang, H. Zheng, P. Adelhelm, T. Brezesinski, P. G. Bruce, M. Danzer, M. El Kazzi, H. Gasteiger, K. B. Hatzell, A. Hayashi, F. Hippauf, J. Janek, Y. S. Jung, M. T. McDowell, Y. S. Meng, P. P. Mukherjee, S. Ohno, B. Roling, A. Sakuda, J. Schwenzel, X. Sun, C. Villevieille, M. Wagemaker, W. G. Zeier and N. M. Vargas-Barbosa, *Nat. Energy*, 2024, **9**, 1310–1320.

28 J. Liu, L. Wang, Y. Cheng, M. Huang, L. Zhao, C. Zheng, W. Li, H. Gao, Z. Li, Z. Wen, G. Luo, Z. Gong, Y. Yang and

M. S. Wang, *Adv. Mater.*, 2025, e2418720, DOI: **10.1002/adma.202418720,**.

29 Y. Xiao, Y. Wang, S.-H. Bo, J. C. Kim, L. J. Miara and G. Ceder, *Nat. Rev. Mater.*, 2019, **5**, 105–126.

30 H. Huo, Y. Bai, S. L. Benz, T. Weintraut, S. Wang, A. Henss, D. Raabe and J. Janek, *Adv. Mater.*, 2025, **37**, e2415006.

31 S. Liang, Y. Sun, Y. J. Cheng, S. V. Roth, P. Müller-Buschbaum, L. Cao, J. Peng, S. Wang, X. Sun and C. Wang, *Adv. Energy Mater.*, 2025, e04045, DOI: **10.1002/aenm.202504045**.

32 A. P. Black, A. Sorrentino, F. Fauth, I. Yousef, L. Simonelli, C. Frontera, A. Ponrouch, D. Tonti and M. R. Palacin, *Chem. Sci.*, 2023, **14**, 1641–1665.

33 Y. Fan, X. Wang, G. Bo, X. Xu, K. W. See, B. Johannessen and W. K. Pang, *Adv. Sci.*, 2025, **12**, e2414480.

34 W. Cheng, M. Zhao, Y. Lai, X. Wang, H. Liu, P. Xiao, G. Mo, B. Liu and Y. Liu, *Exploration*, 2024, **4**, 20230056.

35 K. Luo, M. R. Roberts, R. Hao, N. Guerrini, D. M. Pickup, Y. S. Liu, K. Edstrom, J. Guo, A. V. Chadwick, L. C. Duda and P. G. Bruce, *Nat. Chem.*, 2016, **8**, 684–691.

36 V. Kumar, Nisika and M. Kumar, *Energy Environ. Sci.*, 2021, **14**, 4760–4802.

37 H. Shen, K. Chen, J. Kou, Z. Jia, N. Tamura, W. Hua, W. Tang, H. Ehrenberg and M. Doeff, *Mater. Today*, 2022, **57**, 180–191.

38 H.-K. Tian, A. Chakraborty, A. A. Talin, P. Eisenlohr and Y. Qi, *J. Electrochem. Soc.*, 2020, **167**, 090541.

39 J. M. von Mentlen, M. Fiedler, K. Neumayr, P. Dutta, A. Senol Gungor, S. Dörfler, H. Amenitsch, C. Zaubitzer, H. Althues, V. Wood and C. Prehal, *Batteries Supercaps*, 2025, **00**, e20250042.

40 C. Zhu, T. Fuchs, S. A. L. Weber, F. H. Richter, G. Glasser, F. Weber, H. J. Butt, J. Janek and R. Berger, *Nat. Commun.*, 2023, **14**, 1300.

41 C. Wang, Y. He, P. Zou, Q. He, J. Li and H. L. Xin, *J. Am. Chem. Soc.*, 2025, **147**, 19084–19092.

42 D. Hu, M. L. Beauvais, G. E. Kamm, B. G. Mullens, B. A. Sanchez Monserrate, S. M. Vornholt, P. J. Chupas and K. W. Chapman, *J. Am. Chem. Soc.*, 2023, **145**, 26545–26549.

43 F. M. Alcorn, P. K. Jain and R. M. van der Veen, *Nat. Rev. Chem.*, 2023, **7**, 256–272.

44 X. F. Luo, J. Patra, W. T. Chuang, T. X. Nguyen, J. M. Ting, J. Li, C. W. Pao and J. K. Chang, *Adv. Sci.*, 2022, **9**, e2201219.

45 Y. Nomura, K. Yamamoto, M. Fujii, T. Hirayama, E. Igaki and K. Saitoh, *Nat. Commun.*, 2020, **11**, 2824.

46 M. Sun, T. Liu, Y. Yuan, M. Ling, N. Xu, Y. Liu, L. Yan, H. Li, C. Liu, Y. Lu, Y. Shi, Y. He, Y. Guo, X. Tao, C. Liang and J. Lu, *ACS Energy Lett.*, 2021, **6**, 451–458.

47 X. Zhang, M. Osenberg, R. F. Ziesche, Z. Yu, J. Kowal, K. Dong, Y. Lu and I. Manke, *ACS Energy Lett.*, 2024, **10**, 496–525.

48 Y. Song, Z. Zhou, B. Cui, X. Sun, H. Wang, P. Ji, Q. Liu, H. An, W. Zhao, B. Deng, D. Su and J. Wang, *Angew. Chem., Int. Ed.*, 2025, **64**, e202510172.

49 Q. Liu, Y. Song, R. Gao, C. Fu, H. An, J. Liu, X. Sun, S. Lou, G. Yin, B. Deng, H. Xue, L. Huang and J. Wang, *J. Am. Chem. Soc.*, 2025, **147**, 35244–35254.

50 C. Park, J. Choi, S. Park, H. J. Kim, Y. Kim, G. Lim, J. Lee, E. Lee, S. Jo, J. Kim, J. Kim, J. Lim, T. Kim, J. Hong, D. Kim and S. K. Jung, *Nat. Commun.*, 2025, **16**, 8838.

51 X. Zheng, Z. Xue, H. Hao, Y. Cho, Y. Li, C. Kim, P. Czaja, S. Sanghyun, S. Bone, E. S. Sun, Z. Jiang, X. Wendy Gu, J. N. Weker, G. Yang and J. Nanda, *Sci. Adv.*, 2025, **11**, eady7189.

52 S. Lou, Z. Yu, Q. Liu, H. Wang, M. Chen and J. Wang, *Chem*, 2020, **6**, 2199–2218.

53 J. Wang, Y. C. Karen Chen-Wiegart, C. Eng, Q. Shen and J. Wang, *Nat. Commun.*, 2016, **7**, 12372.

54 W. Li, M. Li, P.-H. Chien, S. Wang, C. Yu, G. King, Y. Hu, Q. Xiao, M. Shakouri, R. Feng, B. Fu, H. Abdolvand, A. Fraser, R. Li, Y. Huang, J. Liu, Y. Mo, T.-K. Sham and X. Sun, *Sci. Adv.*, 2023, **9**, eadh4626.

55 O. Sheng, J. Zheng, Z. Ju, C. Jin, Y. Wang, M. Chen, J. Nai, T. Liu, W. Zhang, Y. Liu and X. Tao, *Adv. Mater.*, 2020, **32**, e2000223.

56 D. Cheng, T. A. Wynn, X. Wang, S. Wang, M. Zhang, R. Shimizu, S. Bai, H. Nguyen, C. Fang, M.-C. Kim, W. Li, B. Lu, S. J. Kim and Y. S. Meng, *Joule*, 2020, **4**, 2484–2500.

57 R. Lin, Y. He, C. Wang, P. Zou, E. Hu, X. Q. Yang, K. Xu and H. L. Xin, *Nat. Nanotechnol.*, 2022, **17**, 768–776.

58 D. Cheng, J. Hong, D. Lee, S. Y. Lee and H. Zheng, *Chem. Rev.*, 2025, **125**, 1840–1896.

59 Q. Wang, H. Xu, Y. Fan, S. S. Chi, B. Han, R. Ke, R. Wang, J. Wang, C. Wang, X. Xu, Z. Zheng, Y. Deng and J. Chang, *Adv. Mater.*, 2024, **36**, e2314063.

60 D. L. R. Melvin, M. Siniscalchi, D. Spencer-Jolly, B. Hu, Z. Ning, S. Zhang, J. Bu, S. Marathe, A. Bonnin, J. Ihli, G. J. Rees, P. S. Grant, C. W. Monroe, T. J. Marrow, G. Li and P. G. Bruce, *Nat. Energy*, 2025, **10**, 1205–1214.

61 Z. Ning, D. S. Jolly, G. Li, R. De Meyere, S. D. Pu, Y. Chen, J. Kasemchainan, J. Ihli, C. Gong, B. Liu, D. L. R. Melvin, A. Bonnin, O. Magdysyuk, P. Adamson, G. O. Hartley, C. W. Monroe, T. J. Marrow and P. G. Bruce, *Nat. Mater.*, 2021, **20**, 1121–1129.

62 J. Kasemchainan, S. Zekoll, D. Spencer Jolly, Z. Ning, G. O. Hartley, J. Marrow and P. G. Bruce, *Nat. Mater.*, 2019, **18**, 1105–1111.

63 S. Hao, S. R. Daemi, T. M. M. Heenan, W. Du, C. Tan, M. Storm, C. Rau, D. J. L. Brett and P. R. Shearing, *Nano Energy*, 2021, **82**, 105744.

64 M. B. Dixit, N. Singh, J. P. Horwath, P. D. Shevchenko, M. Jones, E. A. Stach, T. S. Arthur and K. B. Hatzell, *Matter*, 2020, **3**, 2138–2159.

65 J. A. Lewis, F. J. Q. Cortes, Y. Liu, J. C. Miers, A. Verma, B. S. Vishnugopi, J. Tippens, D. Prakash, T. S. Marchese, S. Y. Han, C. Lee, P. P. Shetty, H. W. Lee, P. Shevchenko, F. De Carlo, C. Saldana, P. P. Mukherjee and M. T. McDowell, *Nat. Mater.*, 2021, **20**, 503–510.

66 M. Sadd, S. Xiong, J. R. Bowen, F. Marone and A. Matic, *Nat. Commun.*, 2023, **14**, 854.

67 W. Li, J. A. Quirk, M. Li, W. Xia, L. M. Morgan, W. Yin, M. Zheng, L. C. Gallington, Y. Ren, N. Zhu, G. King, R. Feng, R. Li, J. A. Dawson, T. K. Sham and X. Sun, *Adv. Mater.*, 2024, **36**, e2302647.

68 A. L. Davis, E. Kazyak, D. W. Liao, K. N. Wood and N. P. Dasgupta, *J. Electrochem. Soc.*, 2021, **168**, 070557.

69 A.-C. Tang, E.-H. Hu, B.-E. Jia, C.-B. Wan, Z.-Y. Wen, S. Tso, X. Ju and Q.-Y. Yan, *Rare Met.*, 2025, **44**, 2268–2293.

70 J. Feijoo, Y. Yang, M. V. Fonseca Guzman, A. Vargas, C. Chen, C. J. Pollock and P. Yang, *J. Am. Chem. Soc.*, 2023, **145**, 20208–20213.

71 O. L. Krivanek, N. Dellby, J. A. Hachtel, J. C. Idrobo, M. T. Hotz, B. Plotkin-Swing, N. J. Bacon, A. L. Bleloch, G. J. Corbin, M. V. Hoffman, C. E. Meyer and T. C. Lovejoy, *Ultramicroscopy*, 2019, **203**, 60–67.

72 L. Pi, E. Björklund, G. J. Rees, W. Song, C. Gong, J.-J. Marie, X. Gao, S. D. Pu, M. Juelsholt, P. A. Chater, J. Park, M. G. Kim, J. Choi, S. Agrestini, M. Garcia-Fernandez, K.-J. Zhou, A. W. Robertson, R. S. Weatherup, R. A. House and P. G. Bruce, *Matter*, 2025, **8**, 101938.

73 G. Greczynski, R. T. Haasch, N. Hellgren, E. Lewin and L. Hultman, *Nat. Rev. Methods Primers*, 2023, **3**, 40.

74 H. Zhang, L. Jeurgens, C. Cancellieri, J. Sivavec, M. V. Kovalenko and K. V. Kravchyk, *ACS Mater. Au*, 2025, **5**, 785–797.

75 B. Aktekin, E. Kataev, L. M. Riegger, R. Garcia-Diez, Z. Chalkley, J. Becker, R. G. Wilks, A. Henss, M. Bär and J. Janek, *ACS Energy Lett.*, 2024, **9**, 3492–3500.

76 R. Dubey, J. Sastre, C. Cancellieri, F. Okur, A. Forster, L. Pompizii, A. Priebe, Y. E. Romanyuk, L. P. H. Jeurgens, M. V. Kovalenko and K. V. Kravchyk, *Adv. Energy Mater.*, 2021, **11**, 2102086.

77 F. de Groot, *Chem. Rev.*, 2001, **101**, 1779–1808.

78 P. Zasimov, L. Amidani, M. Retegan, O. Walter, R. Caciuffo and K. O. Kvashnina, *Inorg. Chem.*, 2022, **61**, 1817–1830.

79 L. Bugarin, H. A. Suarez Orduz and P. Glatzel, *J. Synchrotron Radiat.*, 2024, **31**, 1118–1125.

80 W. Yang and T. P. Devereaux, *J. Power Sources*, 2018, **389**, 188–197.

81 Y. Gu, J. Barker, J. Li, T. Kikkawa, F. Camino, K. Kisslinger, J. Sinsheimer, L. Lienhard, J. J. Bauer, C. A. Ross, D. N. Basov, E. Saitoh, J. Pelliciari, G. E. W. Bauer and V. Bisogni, *Nature*, 2025, **645**, 900–905.

82 F. M. F. de Groot, M. W. Haverkort, H. Elnaggar, A. Juhin, K.-J. Zhou and P. Glatzel, *Nat. Rev. Methods Primers*, 2024, **4**, 45.

83 Z. Wang, D. Santhanagopalan, W. Zhang, F. Wang, H. L. Xin, K. He, J. Li, N. Dudney and Y. S. Meng, *Nano Lett.*, 2016, **16**, 3760–3767.

84 A. E. Goode, A. E. Porter, M. P. Ryan and D. W. McComb, *Nanoscale*, 2015, **7**, 1534–1548.

85 J. L. Hart, A. C. Lang, Y. Li, S. Shahrezaei, D. D. Alix-Williams, M. L. Falk, S. N. Mathaudhu, A. I. Frenkel and M. L. Taheri, *Mater. Today Nano*, 2023, **21**, 100298.

86 L. An, J. Swallow, P. Cong, R. Zhang, A. Poletayev, E. Bjorklund, P. Didwal, M. Fraser, L. Jones, C. Phelan, N. Ramesh, G. Harris, C. Sahle, P. Ferrer, D. Grinter, P. Bencok, S. Hayama, M. S. Islam, R. House, P. Nellist, R. Green, R. Nicholls and R. Weatherup, *Energy Environ. Sci.*, 2024, **17**, 8379–8391.

87 Y. Zheng, L. Hu, W. Li, T. Huang, J. Ma, S. Dong and G. Cui, *ACS Energy Lett.*, 2024, **9**, 5296–5309.

88 G. Liang, C. Zhang, L. Yang, Y. Liu, M. Liu, X. Xiong, C. Yang, X. Lv, W. You, K. Pei, C. J. Zhong, H. W. Cheng and R. Che, *Nano-Micro Lett.*, 2025, **17**, 245.

89 S. Lee, H. Park, J. Y. Kim, J. Kim, M. J. Choi, S. Han, S. Kim, W. Kim, H. W. Jang, J. Park and K. Kang, *Nat. Commun.*, 2024, **15**, 7947.